Rheological evaluation of soil aggregate microstructure and stability across a forested catena

Published in Geoderma
https://doi.org/10.1016/j.geoderma.2021.115196

Authors:

F. Javaheri
Ph.D. student of Soil Science Department, College of Agriculture,
Vali-e-Asr University of Rafsanjan, Rafsanjan, Iran
Email: f.javaheri@stu.vru.ac.ir

I. Esfandiarpour-Boroujeni
Associate prof. of Soil Science Department, Faculty of Agriculture,
Vali-e-Asr University of Rafsanjan, Rafsanjan, Iran
Email: esfandiarpoor@vru.ac.ir

H. Kourki
Assistant prof. of Chemistry and Chemical Engineering Department,
Graduate University of Advanced Technology, Kerman, Iran
Email: hajir.kourki@kgut.ac.ir

M. H. Farpoor
Professor of Soil Science Department, Faculty of Agriculture,
Shahid Bahonar University of Kerman, Kerman, Iran
Email: farpoor@uk.ac.ir

R. D. Stewart
Associate prof., School of Plant and Environmental Sciences, Virginia Tech. University,
Blacksburg, VA, USA
Email: ryan.stewart@vt.edu

Corresponding Author:

R. D. Stewart
Associate prof., School of Plant and Environmental Sciences, Virginia Tech. University,
Blacksburg, VA, USA
Email: ryan.stewart@vt.edu

Rheological evaluation of soil aggregate microstructure and stability across a forested catena

Abstract

Rheological characteristics of soils, including their deformation and flow behaviors when subjected to external stress, can provide important information on microstructural stability. In this study we used rheological measurements to examine the soil aggregate microstructure and stability of four different soil orders – Alfisol, Mollisol, Inceptisol, and Entisol – along a forested catena in Mazandaran Province, northern Iran. Amplitude sweep tests were used to quantify the initial values of the storage and loss moduli, deformation limit (when the material begins to transition from reversible to irreversible deformation), deformation at flow point (when the material becomes viscous), and *integral z* (which summarizes the overall visco-elasticity of the material). The deformation limit was significantly higher in subsoil layers than topsoil layers, and was also higher in the Mollisol than the other pedons. The flow point and *integral z* values, which relate to the structural stiffness of soil matrices, were largest in the Btg horizons of the Alfisol and Mollisol, implying that these soils had more rigid microstructures. In contrast, the Entisol Ckg horizon, which had high sand content and little soil development, had the lowest values for all properties, thus indicating a lack of micro-aggregate stability. Regression analyses revealed that *integral z* was influenced by soil physicochemical properties, and was higher in soils whose clay fraction was dominated by expansive clay minerals and pedogenic iron and aluminum sesquioxides. Altogether, the rheological parameters indicated that older, more developed soils had greater microstructural stability than their less developed counterparts. As a result, rheological measurements may be useful for identifying the major factors that affect soil aggregation, and can indicate the relative amount of soil development along gradients such as the studied forest catena.

Keywords: Rheology; Deformation; Amplitude sweep test; Soil development; soil organic carbon (SOC)

1. Introduction

Soil aggregate stability, which describes the resistance of particle associations against externally applied stresses – including water and wind erosion, shrinking and swelling processes, or tillage (Le Bissonnais, 1996; Guo et al., 2019) – is a key indicator of soil physical quality. Soil aggregation is often associated with improved structure (Six et al., 2000b) and changes in other properties such as bulk density (Six et al., 2004). Conversely, soil aggregates that lack adequate stability can experience slaking during wetting. This process can destroy soil structure, which in turn can increase erosion potential and decrease water infiltration rate due to pore-clogging (Jastrow and Miller, 1991). Further, because soil aggregate stability influences both soil properties and environmental fluxes (e.g., water infiltration and atmospheric gas exchange), it plays an important role in the rate and extent of soil formation.

Soil aggregate stability is highly sensitive to the soil properties and management (Abid and Lal, 2009), and often reflects the impacts of land use (Castro Filho et al., 2002). At a micro-scale, aggregate stability varies based on the strength of forces such as hydrogen bonds within water menisci, covalent bonds within organo-mineral interactions, and ionic forces (Ghezzehei and Or,

2001; Baumgarten et al., 2012; Buchmann and Schaumann, 2017). Aggregates often form in a hierarchical manner, with smaller "micro-aggregates" representing the relatively stable building blocks of larger "macro-aggregates" (Six et al., 2004; Gyawali and Stewart, 2019). These micro-aggregates can be important reservoirs of soil carbon (Skjemstad et al., 1990; Six et al., 2000a), making it important to understand the mechanisms by which these aggregates form and persist.

Landscape position represents one potentially important factor affecting the formation and persistence of soil micro-aggregates. A hillslope catena is a landscape unit in which soils derived from a single parent material under similar climatic conditions gain different characteristics due to variations in relief and related processes such as drainage, differential transport and deposition of eroded materials, and leaching and translocation of mobile chemical constituents (Schaetzl and Anderson, 2005; Pasquini et al., 2017; Rosemary et al., 2017). Internal drainage and duration of saturation (i.e., waterlogging) typically vary along a given catena, with low-lying areas often wetter than those above (Schaetzl and Anderson, 2005). Over time, these processes can cause soil pedons to vary in their genetic and diagnostic horizons, depth, assemblages, and structure. It stands to reason that such pedon-scale differences will be associated with variations in soil micro-aggregate stability, though the exact nature of these relationships remains poorly understood.

Methods typically ascribed for measuring aggregate stability – such as wet sieving (Yoder, 1936) or Cornell sprinkler analysis (Van Es and Schindelbeck, 2003) – focus on the larger, macro-sized aggregates, and therefore provide little information on micro-sized aggregates (e.g., < 0.25 mm in size). More recent methods have used total aggregate size distributions to measure the proportion of micro-aggregates within soil samples (e.g., Gyawali and Stewart, 2019). None of these approaches, however, assess the conditions under which aggregates are stable or the amount of deformation that aggregates can withstand. In contrast, rheometry can be used to assess the elastic versus plastic behavior of soils across a range of deformation, and thereby provide a more quantitative interpretation of micro-aggregate susceptibility or resistance to failure (Baumgarten et al., 2012 and 2013; Keller et al., 2013). Fundamental concepts of soil rheology have also been used to describe flow behaviors and time-dependent stress-strain relations (Ghezzehei and Or, 2001).

The amplitude sweep test (AST) was developed to assess microstructural stability and viscoelastic behaviors of soils (Mezger, 2006; Holthusen et al., 2010; Khitrov and Khaydapova, 2019). For example, AST has been used to identify soil structural changes resulting from the use of fertilizers and biochar amendments (Baumgarten et al., 2012; Holthusen et al., 2012; Ajayi et al., 2016; Ajayi and Horn, 2017). These studies found that higher concentrations of organic compounds and polyvalent cations such as Ca^{2+} were associated with a wider range of elastic behavior and a higher deformation limit (i.e., the strain at which the material begins to plastically deform). AST has also been used to test variations in micro-aggregate stability in soils with varying particle-size distributions (Markgraf and Horn, 2006), mineralogical compositions (Ghezzehei and Or, 2001; Or and Ghezzehei, 2002; Markgraf et al., 2009), soil water content and potential (Holthusen et al., 2012; Markgraf et al., 2012; Pertile et al., 2016), and concentrations of salts and other exchangeable ions in the soil solution (Baumgarten et al., 2012; Javaheri et al., 2021).

Besides, this approach has been used to study the microstructural changes and stiffness degradation in Oxisols and Vertisols in Brazil (Markgraf and Horn, 2007) and Fluvisols in Germany and Spain (Markgraf et al., 2012; Baumgarten et al., 2013; Stoppe and Horn, 2018).

Despite the growing use of rheological characterizations in soil science, few studies have used rheometry to evaluate specific interactions between soil micro-aggregate stability, pedology, and related physicochemical soil properties. Moreover, no study has examined the soil micro-aggregate stability of different soil types in forest soils of Iran. The aim of this study, therefore, was to investigate soil aggregate microstructure and stability or micro-aggregate stability along a catena in Kheyrud forest, Mazandaran Province, northern Iran. The study used a combined pedological-rheological approach to better understand specific soil properties that correlate with greater micro-aggregate stability. The results should be useful to others interested in evaluating and predicting soil micro-aggregation along gradients in soil development.

2. Theory

The total soil strain rate can be divided into elastic and viscous components, with the ratio of elastic to viscous strain dependent on the stress rate and loading time (Ghezzehei and Or 2001; Keller et al., 2013). These components can also be combined to define soil as a viscoelastic substance, characterized by a modulus G [M L^{-1} T^{-2}]:

$$G = \frac{\tau_c}{y_c} \tag{1}$$

where τ_c is the applied shear stress [M L^{-1} T^{-2}] and y_c is the corresponding shear strain [L L^{-1}] (Markgraf, 2011).

The total modulus can be further divided into two terms: a storage modulus, G′ [M L^{-1} T^{-2}], and a loss modulus, G″ [M L^{-1} T^{-2}]. G′ describes the energy stored by a sample during the deformation process and thereby accounts for elastic behavior, while G″ is a measure of the energy lost during deformation of a sample due to inner friction, and thereby describes the viscous behavior of the soil. These two terms can be determined by the amplitude sweep test (AST), in which an oscillating plate imposes a series of controlled shear rates on the sample.

A representative result of an AST is shown in Figure 1. The loss factor, tan δ, is calculated as the ratio of G″ to G′. It, therefore, quantifies the real part of the dissipating energy of deformation γ (Markgraf, 2011; Baummgarten et al., 2012). The loss factor can also help to identify three phases of elasticity loss as follows (Figure 1):

Phase 1 – Initial or stored elasticity (sometimes also called the “gel” state), in which tan $\delta < 1$ and does not change with increasing deformation. In this quasi-elastic phase, applied deformation leads to full microstructure recovery, which is represented by a spring for ideal elastic substances (Hooke’s law). The quasi-elastic stage is also referred to as the linear viscoelastic range (LVE), and its upper bound is the deformation limit (γ_L).

Phase 2 – Stage of pre-flowing or transgression, in which tan $\delta < 1$ and increases with increasing deformation. In this phase, the material transitions between elastic and plastic behaviors as soil particles become re-oriented, and microstructural stability decreases. In the transgression phase, reversible and irreversible deformation both occur, meaning that the strain is time-dependent and

not fully recoverable (Malkin and Isayev, 2017). The upper bound of this phase is tan δ = 1, i.e., the flow point (γ_f). At this point, G′ = G″ and the elastic and viscous parts are equivalent, and increasing deformation will irreversibly destroy the microstructure.

Phase 3 – The final stage of structural collapse, in which tan δ > 1. In this phase viscous behavior occurs, and microstructural collapse and soil deformation are irreversible, as represented by ideal fluids following Newton's law of viscosity (Mezger, 2006; Markgraf and Horn, 2007).

For further comparison of the quasi-elastic range (tan δ < 1), the dimensionless area parameter *integral z* is defined according to Stoppe and Horn (2018):

$$\int_0^{\gamma_f}(1-\tan\delta)d\gamma \qquad (2).$$

Greater values of *integral z* are associated with more elastic and rigid materials. Therefore, *integral z* describes the structural strength in consideration of elasticity loss due to increasing shear deformation γ over time (Figure 1).

3. Materials and methods

3.1. Site description

A catena was selected in the Kheyrud Hyrcanian forest of northern Iran along the southern coast of the Caspian Sea (Figure 2). The catena is located 7 km east far from Nowshahr, Mazandaran Province, Iran (36° 36′ N; 51° 33′ E), with an elevation ranging from 30 to 420 m above mean sea level (asl). The area has a humid subtropical climate pattern with mild winters (based on the Köppen-Geiger climate classification system; Kottek et al., 2006), mean annual temperature of 16.2 °C (mesic regime), mean precipitation of 1303 mm, and a udic/aquic soil moisture regime. The main parent materials are Mesozoic-Cretaceous limestone, especially argillaceous limestone (Geological Survey of Iran, 1995). The vegetation types of the area vary from the deciduous broad-leaved forest and mixed forest with *Carpinus betulus*, *Ulmus glabra*, *Acer velutinum*, and *Alnus subcordata*.

3.2. Soil sampling and laboratory analysis

We excavated four representative pedons along the catena in fall 2017 (Figure 2). The pedons were described based on the "Field Book for Describing and Sampling Soils" (Schoeneberger et al., 2012) and were classified to the subgroup level as 1) Aeric Endoaqualfs, 2) Aquic Argiudolls, 3) Oxyaquic Eutrudepts, and 4) Mollic Endoaquents, according to U.S. Soil Taxonomy (Soil Survey Staff, 2014). Soil samples were collected from the genetic horizons of the pedons, air-dried, ground, and passed through a 2-mm sieve. Percentage of the coarse fragments (CF) was determined by sieving, particle size distribution by pipette method, calcium carbonate equivalent (CCE) by titration (Nelson, 1982), electrical conductivity (EC) by measuring a saturated extract, soil pH using a saturated paste (Jackson, 1958), soil organic carbon (SOC) content using the oxidation method (Walkley and Black, 1934), cation exchange capacity (CEC) by the Bower method (Sumner and Miller, 1996), bulk density (Bd) and porosity by analyzing volumetric cores (Martin et al., 2017), water content by oven drying (Rhoades, 1996), redox potential (i.e., reducing condition, rH) using a standard hydrogen electrode (Husson, 2013), and soluble Ca^{2+} in saturation extract by atomic absorption spectrophotometry (Richards, 1954). In addition, acid ammonium

oxalate extractable iron and aluminum (i.e., Fe_o and Al_o), and dithionite-citrate extractable iron (i.e., Fe_d) were determined according to Mehra and Jackson (1958). Atomic absorption was used for Fe and Al determination of extracts using a SAvantAA (GBC Scientific Equipment, Braeside, VIC, Australia). Water contents were expressed as saturation percentages by dividing volumetric water content by total porosity. Three samples were analyzed for each horizon (n = 3).

3.3. Clay mineralogy analysis

X-ray diffraction (XRD) was performed on the clay-size fraction with a computer-controlled Siemens D5000 (Kittrik and Hope, 1963). All XRD patterns were recorded on a Bruker D8 X-ray diffractometer equipped with CuKα radiation (λ = 0.15418 nm). The diffractometer operated at a tube current of 40 mA and a voltage of 40 kV. The analysis used 2θ angles from 3 to 30°, with a step size of 0.02° and a scan speed of 1° min^{-1}. Clays were randomly oriented on glass slides, and subjected to standard treatments: Mg-saturation, Mg-saturation with glycerol solvation, K-saturation (25 °C), and heat treatment of the K-saturated slides at 550 °C. The identification of clay minerals was done by comparing diffractograms and following the approach of Dixon and Weed (1989). One XRD analysis was performed for each soil genetic horizon.

3.4. Rheometry analysis

We selected a subset of the sampled horizons to perform rheological measurements. Here our goal was to compare rheological properties at similar depths across the four pedons, similar to the approach of Baumgarten et al. (2012). Therefore, we took soil samples from the 10 cm and 40 cm depths (all pedons) along with the 80 cm depth (Pedon 3). The 10 cm depth samples corresponded to A or AB horizons, and therefore was considered to represent the topsoil layers. The 40 cm depth samples corresponded to Bt or Bw horizons in Pedons 1-3, and the C horizon in Pedon 4, and the 80 cm depth sample from Pedon 3 was chosen to provide a representing Bw horizon as part of the analysis (and thereby provide data on a genetic horizon commonly found in this region). The 40 and 80 cm depth samples were considered to represent subsoil layers.

We equilibrated all samples at a quasi-saturated state with a uniform distribution of the water. We then used the following sample preparation procedure: homogenized soil samples were sieved through 2-mm mesh and repacked to a standard bulk density (Bd = 1.3 g cm^{-3}) within small cylinders (2.5 cm diameter and 1.0 cm height). They were then capillary saturated with distilled water, with a water potential of 0 kPa at the bottom where the cylinder contacted the water table. Thereafter, a small amount of soil was taken out of each cylinder with a spatula and was placed on the measuring plate of a Discovery Hybrid Rheometer-3 (DHR-3; TA Instruments, New Castle, DE, USA) without any mechanical disturbance (Figure 3).

Rheometric measurements were performed on three physical samples per horizon (n = 3). The rheometer was equipped with a parallel-plate measuring system with 25 mm diameter plates separated by a 4-mm distance (Markgraf and Horn, 2007). For each replicate, an amplitude sweep test (AST) was carried out at 25 °C with controlled shear deformation (logarithmic range or γ = 0.0001-100 %) ~~followed by a frequency sweep test and the resting period of 30 seconds between measurement points~~. The frequency was set at a constant value of f = 0.5 Hz (angular frequency, $\omega = \pi\ s^{-1}$). Following Baummgarten et al. (2012), any excess material beyond the plate perimeter

was left in place during the run to mitigate any effect from possible drying at the lateral edges. The test continued until 30 points were collected, with each run lasting approximately 8 min for A horizons samples and 10 min for B horizons samples. The normal force on the samples always exceeded 14 N at the beginning of the test and went to 0 N by the end of the test.

The TRIOS/v5.1.0 software program (TA Instruments, New Castle, DE, USA) and MATLAB/v8.1.347 (Mathworks, Natick, MA, USA) were used to calculate γ_L, and γ_f, and *integral z*. Due to excessive noise at low deformation, the initial elastic modulus (i.e., G'_0) and initial loss modulus (i.e., G''_0) values were estimated at the deformation closest to 0.001%; we then assumed these moduli were constant through the deformation range $0 < \gamma < 0.001\%$ when estimating *integral z*. Deformation limit γ_L was identified as the deformation when G' first deviated >5% from G'_0. Flow point γ_f was identified as the deformation when $G' = G''$. We ran multiple ASTs on some of the replicates, in which case we used the mean value for each parameter in our statistical analysis.

3.5. Statistical analysis

Means and standard deviations were calculated for all rheometric and physicochemical properties for each horizon. The rheometric parameters G'_0, G''_0, γ_L, and γ_f, and *integral z* were compared using a two-way ANOVA with soil order and horizon (topsoil versus subsoil) as factors and $\alpha = 0.05$. G'_0 and G''_0 were log-transformed prior to analysis. The rheological parameters were also compared against measured SOC, Ca^{2+}, Fe_d, Fe_o, Al_o, and clay percentage using linear regression. Regressions were performed for topsoil horizons (using the mean values from each pedon for the 10 cm depth) and subsoil horizons (using the mean values from each pedon for the 40 cm and 80 cm depths). Regression relationships were evaluated for significance assuming an alpha value of 0.1. Statistical analyses were performed using R (Windows Version 4.0.3) and EXCEL/v.365 (Microsoft Corporation, Redland, WA, USA).

4. Results

4.1. Physicochemical and mineralogical properties of soils

Table 1 shows a summary of the physicochemical and morphological properties of studied soils. The EC contents of all soils were low (0.430 to 0.877 dS m^{-1}). The Mollisol pedon had the lowest CCE (0.2 to 3.1 %) while the Entisol pedon had the highest CCE (18.8 to 32.0 %). The mean percentage of SOC ranged from 0.5 % in the Bg horizon of the Inceptisol to 13.6 % in the Oi horizon of the Mollisol. The CEC contents were different between soils and horizons, with the Ckg1 horizon in the Entisol having the lowest (16.4 $cmol_+$ kg^{-1}) and the 2Bw2 horizon in the Inceptisol having the highest (31.3 $cmol_+$ kg^{-1}) values. Soil pH ranged from slightly acidic to neutral. The minimum Ca^{2+} concentration occurred in the Ckg1 horizon of the Entisol (7.8 mmol l^{-1}) and the maximum value was in the Bg2 horizon of the Inceptisol (16.3 mmol l^{-1}). The Bd values ranged between 0.61 g cm^{-3} (Oi horizon of the Mollisol) to 1.69 g cm^{-3} (Bg2 horizon of the Inceptisol). The Fe_d varied from 2.5 g kg^{-1} (Ckg1 horizon of the Entisol) to 18.2 g kg^{-1} (Oi horizon of the Mollisol). The Fe_o+Al_o content was higher in the 2Bw horizons of the Inceptisol than all other studied horizons (Table 1). Redoximorphic features were observed in all subsoil (i.e., B and

C) horizons, along with the A horizon in the Alfisol. Many of those horizons also had evidence of reducing conditions, as indicated by rH values that varied from 14.8 (Btg1 horizon of the Mollisol) to 22.4 (Ckg1 horizon of the Entisol). The most common type of soil structure in the area was subangular blocky. The soil texture of the studied pedons also varied from medium (e.g., loam) to fine (e.g., clay).

Semi-quantitative analysis of clay minerals determined that the soils of the studied pedons had different clay minerals, including kaolinite, vermiculite, smectite, illite, chlorite, and quartz (Table 2). The Alfisol was characterized as having a high percentage of kaolinite (≥25%) and a moderate amount of smectite and vermiculite (10-25%) in all genetic horizons. The Mollisol was dominated by vermiculite in the AB horizon and smectite in the Btg horizons, with moderate amounts of kaolinite, vermiculite, and illite in all horizons. The Inceptisol had a high concentration of kaolinite in its A1 and A2 horizons, kaolinite along with a moderate amount of smectite in its Bg1 and Bg2 horizons, and kaolinite and smectite in its 2Bw1 and 2Bw2 horizons. Finally, the Entisol had moderate amounts of kaolinite, vermiculite and illite in its A horizon, with predominantly quartz in its Ckg1 and Ckg2 horizons.

4.2. Rheological properties

The initial stored elasticity phase (Phase 1) was well defined for all soil horizons (AST results for samples with median G′ and G″ values are shown in Table 3 and Figure 4). However, the initial values of G′ and G″ differed among soil orders. The Mollisol and Inceptisol, along with the Btg2 horizon of the Alfisol, had the highest storage and loss moduli, with G'_0 from 5,000 kPa to 8,000 kPa and G''_0 values from 500 to 2,000 kPa. Horizons in the Entisol had much lower initial modulus values, with G'_0 between 50 and 30 kPa and G''_0 between 10 and 70 kPa. Furthermore, the pedons varied in their relative modulus values between layers: the subsoil horizons in the Alfisol and Mollisol had higher G'_0 and G''_0 compared to their topsoil counterparts, whereas the opposite was observed for the Inceptisol and Entisol, as those soils had higher G'_0 and G''_0 in its topsoil compared to its subsoil.

The ratio of modulus values (i.e., G''_0/G'_0) was used to quantify the loss factor (i.e., tan δ) as a function of deformation from shear stress (Figure 5). All samples showed curve characteristics that indicated rigid microstructures, with fully elastic characteristics for all samples (i.e., Phase 1) when γ was less than 0.1 %. An increase of tan δ was then evident at γ = 0.01-1 % in all horizons, as the soils entered Phase 2. The samples reached tan δ = 1 (flow point) at deformations from 10 – 100 %, after which point the microstructure collapsed (Phase 3). The topsoil samples (A and AB horizons) showed a steeper increase in tan δ, resulting in an earlier intersection with the tan δ = 1 (Figure 5a). Subsoil samples required greater deformation to reach tan δ =1 and had more gradual slopes, except the Ckg1 horizon of the Entisol. In contrast, the Btg horizons of the Alfisol and Mollisol both exhibited a gradual decrease of microstructure for the entire deformation range (Figure 5b).

Translating the AST curves into rheological parameters (Table 3) revealed other distinctions between pedons and soils. For instance, the topsoil layers had lower values for deformation limit, γ_L, than the subsurface layers ($p < 0.001$). The γ_L values were similar in the A horizons of Pedons

1, 3, and 4 (0.012 to 0.014%), and also in the B horizons of those pedons (0.023 to 0.032%). However, the Mollisol had significantly higher mean γ_L values (0.024 % in its AB horizon and 0.041 % in its Btg horizon) compared to the other pedons ($p < 0.05$). Note that the interaction between pedon and layer was not significant for that parameter ($p = 0.19$).

The flow points (γ_f) significantly varied by both pedon and topsoil versus subsoil layer ($p < 0.001$). The Mollisol had significantly higher γ_f in its subsoil (55.2 ± 6.4 %) compared to its topsoil (22.7 ± 4.2 %), whereas the other pedons did not have significant differences in their topsoil versus subsoil values. The A horizon of the Alfisol had a significantly higher mean γ_f than the A2 horizon of the Inceptisol (33.6 % versus 11.7 %), but the other topsoil values were statistically similar to both. For the subsurface horizons, the Alfisol and Mollisol had significantly higher γ_f values than the Inceptisol and Entisol in the subsoil, with the Entisol having a significantly smaller γ_f than the Inceptisol (the latter with a mean of 4.2 % compared to 18.0 and 22.4 % for the former).

The *integral z* values also significantly varied both by pedon and in topsoil versus subsoil layers ($p < 0.001$). The Btg horizons of Pedons 1 and 2 had higher values than the other horizons, with means of 68.3 ± 6.2 (Alfisol) and 82.8 ± 7.3 (Mollisol). The AB horizon in the Mollisol also had a larger *integral z* (28.0 ± 6.2) than the Ckg1 horizon in the Entisol (7.2 ± 1.2). All other horizons had *integral z* values that were similar in magnitude, on the order of 10-20.

4.3. Correlations among *integral z*, OC, Fe_d, Al_o, Ca^{2+}, and clay content

Figure 6 presents linear regressions between *integral z* and SOC, Ca^{2+}, Fe_d, Fe_o, Al_o, and clay percentage. The SOC content was negatively correlated to *integral z* (Figure 6a), with $R^2 = 0.31$ in the topsoil layers and 0.21 in the subsurface horizons. Calcium concentrations were positively correlated with *integral z* (Figure 6b), though the relationships were very weak, with $R^2 = 0.02$ in the topsoil and 0.16 in the subsoil. Relatively strong positive correlations were found for *integral z* with Fe_d ($R^2 = 0.84$ in topsoil and 0.95 in subsoil; Figure 6c) and Al_o ($R^2 = 0.90$ in topsoil and 0.72 in subsoil; Figure 6e), though the correlation was not as strong for Fe_o ($R^2 = 0.29$ in topsoil and 0.46 in subsoil; Figure 6d). Clay percentage was the only parameter where the direction of the correlation varied between topsoil and subsoil samples, with topsoil showing a negative correlation (with $R^2 = 0.06$) and subsoil showing a positive one (with $R^2 = 0.20$; Figure 6f). The relationships between *integral z* and Fe_d and Al_o were significant ($p < 0.1$) for both topsoil and subsoil samples, whereas the other relationships were not significant.

5. Discussion

Micro-aggregate stability is associated with improvements in soil properties (Boix-Fayos, et al., 2001) and can facilitate long-term soil carbon sequestration (Skjemstad et al., 1990; Six et al., 2000a). In this study we tested the ability of rheological parameters determined via amplitude sweep tests (ASTs) to quantify differences in micro-aggregate structure and stability. Analyzed properties included G'_0 (initial storage modulus) and G''_0 (initial loss modulus), γ_L (deformation limit), γ_f (flow point), and *integral z*. The study results indicated that soil micro-aggregate strength varied between topsoil versus subsurface soil horizons, and also between soil pedons with different

properties and degrees of development. For instance, the Mollisol pedon had higher γ_L than the other soils. Higher γ_L values indicate a wider range of Phase 1 deformation range, in which the material undergoes reversible elastic strain (Markgraf et al., 2006). Also, the Alfisol and Mollisol samples demonstrated the widest range of deformation via transgression (i.e., Phase 2) due to their high γ_f values, particularly in the subsoil layers. Large γ_f values indicate quasi-stable arrangements of soil particles (Dexter, 1988). The Inceptisol and Entisol samples, by contrast, exhibited rapid transitions between Phases 1 and 2 (e.g., Figure 4c) and relatively low γ_f. In particular, the Ckg horizon of the Entisol showed less resistance to deformation by having the lowest γ_f. Since that horizon was composed of undeveloped parent material (e.g., massive soil structure), this result suggests that γ_f may be correlated with the soil development rate.

The pedons also differed in their initial modulus values. The Mollisol and the Inceptisol, along with the Btg2 horizon of the Alfisol, had relatively large G'_0, while the Entisol exhibited the lowest values for G'_0. High elastic modulus (G') indicates greater resistance to deformation and a higher rigidity, which helps to determine soil quality and directly influences soil aggregation stability (Baumgarten and Horn, 2013). However, the same patterns were also observed for initial loss modulus (G''_0) values, wherein the Mollisol and the Inceptisol and the subsoil in the Alfisol had higher values than the other layers. Higher values of this loss term indicate that the material behaves as a viscous fluid rather than an elastic solid, and therefore becomes plastically deformed during strain. As a result, the different soils had similar initial tan δ values, ranging from 0.1 to 0.3 (Fig. 5). We also quantified the relative proportion of the elastic G' to plastic G″ terms under increasing strain, as indicated by the tan δ curves. The test results showed a fairly consistent increase in tan δ between γ of 0.01 and 1 % (Figure 5), indicating that G″ increased at a consistently higher rate than G′. This behavior was likely due to the reorientation of soil particles such as kaolinite platelets, individual packages, or grains (Markgraf and Horn, 2007). Then, when deformation varied from γ of 1 to ~10 %, the tan δ values tended to stabilize, particularly in the topsoil samples. This stabilization likely reflected a relative shift from viscosity towards elasticity as the particles re-stabilized in new positions (Markgraf et al., 2006).

As discussed above, it is necessary to consider both storage and loss moduli together when interpreting rheological measurements. To this end, the *integral z* parameter may be the most useful indicator of micro-structural stability. This term effectively quantifies the excess of elastic to plastic deformation across a range of soil strain (Baumgarten et al., 2013 and Stoppe and Horn, 2018). It therefore encompasses the other rheological parameters included in this study (i.e., γ_L, γ_f, G'_0, G''_0). The ANOVA comparison for *integral z* showed that the Btg horizons in Pedons 1 and 2 had greater microstructural stability than other horizons (Table 3). Conversely, the Ckg1 horizon in the Entisol had the lowest *integral z*, with significant differences from the Mollisol and Inceptisol. Overall, layers with subangular blocky structure tended to have relatively high *integral z* values, whereas the horizons with granular or massive structure had relatively low values (e.g., mean < 18). Previous studies have determined that aggregates with blocky structure often exhibit rolling shear behavior (i.e., shear stress perpendicular to aggregates), whereas more platy or massive structure leads to sliding shear behavior that translates to greater soil strain (Smith and

Reitsma, 2002; Cho et al., 2006). The different *integral z* values measured in our study may therefore signify the importance of soil structure in helping aggregates resist deformation and collapse.

We also used *integral z* as the master response variable for testing correlations with other physicochemical properties. The resulting linear regressions provided insights into how different physicochemical properties influence microstructural stability. For instance, higher Fe-Al oxide/hydroxide (i.e., sesquioxide) concentrations were associated with larger *integral z* values for both topsoil and subsoil horizons (Figs. 6c-6e). The correlation between Al_o content of the top soil and *integral z* was notably strong ($R^2 = 0.90$), as was the correlation between *integral z* and Fe_d content of the subsoil ($R^2 = 0.96$). Previous research has indicated that the formation of aluminum oxide complexes with organic compounds can lead to flocculation and aggregate stability in near-surface soils (Mbagwu and Schwertmann, 2005; Baumgarter et al., 2013). At the same time, other studies have identified Fe oxides as being often the most important stabilizing factor in many soils (e.g., Muggler et al., 1999), with iron redox cycling and conversion of ferrihydrite to hematite acting as factors that increase aggregate stability (Ohstubo et al., 1991). In our study, the soil horizons with largest *integral z* values (i.e., Btg2 horizon in the Alfisol and Btg1 horizon in the Mollisol) had clear redoximorphic features and rH<20, which is considered to be an indication of aquic conditions (IUSS WRB, 2015).

Iron oxide structure can also be important, as seen here by the significant relationship between *integral z* and Fe_d, but not between *integral z* and Fe_o. The oxalate extraction method associated with Fe_o values releases organic-bound and amorphous iron oxides, whereas the dithionite-citrate extraction associated with Fe_d values also includes crystalline Fe oxides (McKeague and Day, 1966; Levine and Ciolkosz, 1983; Walker, 1983; Asgari et al., 2018). While some studies have determined that amorphous minerals can provide substantial aggregate stability when forming complexes with organo-molecules (e.g., Pinheiro-Dick and Schwertmann, 1996; Duiker et al., 2003), other work has identified crystalline iron content as being far more important (Igwe et al., 2013; Wang et al., 2016; Goebel et al., 2017). Our results provide support to the latter group of studies, supplying additional evidence that crystalline iron oxides contribute more to micro-aggregate stability than do amorphous forms of iron. At the same time, the relative content of crystalline to amorphous sesquioxides tends to increase as soils age (Walker, 1983). Therefore, the strong relationship between *integral z* and Fe_d seen here suggests that the more developed pedons in our study had greater micro-aggregate stability than their less developed counterparts.

Clay content is another factor that can influence microstructural stability and soil elasticity (Holthusen et al., 2010). In our study, however, clay content had a non-significant and inconsistent relationship with *integral z* (Figure 6f). Specifically, the subsoil samples showed a positive correlation between the two parameters, whereas the topsoil samples showed a negative correlation. One reason for the discrepancy could be that the studied pedons had distinct mineralogies, with different amounts of smectite, kaolinite, vermiculite, illite, and quartz (Table 2). Previous work has suggested that soils with dominant kaolinite clay mineralogy tend to be less elastic (Markgraf and Horn, 2007), as indicated here by the lower *integral z* values measured in

the sandy loam and silty loam soils of the Inceptisol and Entisol. At the same time, the Btg2 horizon in the Alfisol and the Btg1 horizon in the Mollisol had moderate to dominant amounts of 2:1 smectite and vermiculite phyllosilicates, which can increase shear resistance of the soils as indicated by larger LVE ranges (Holthusen et al., 2010). Previous work in southern Brazil indicated that Vertisol soils with high smectite content had increased γ_L compared to nearby Oxisols and Ultisols (Pértile et al., 2018). Therefore, proper understanding of rheological properties may require assessing both the type and overall content of clay minerals.

Soil organic matter and exchangeable cation type can also be important factors for micro-aggregate stability. For example, previous work has suggested that SOC, by acting as a strong binding agent, can increase soil elasticity (Holthusen et al., 2012; Pértile et al., 2017). However, our correlation analysis showed that *integral z* was negatively correlated with SOC content (Figure 6a). There are a couple of possible mechanisms that may explain these results. For one, in some soils SOC can increase particle dispersion if bound to positively charged functional groups on clay minerals (Stoppe and Horn, 2018). For another, soils with high organic matter content can have relatively high saturated water contents and relatively low bulk densities (Pértile et al., 2016), both of which factors can reduce soil strength to shear stress (Ghezzehei and Or, 2001; Stoppe and Horn, 2018). Therefore, even though all samples were quasi-saturated at the time of analysis, it is possible that differences in saturated water contents may have influenced the rheological measurements. In terms of pore water chemistry, "bridging" divalent cations such as Ca^{2+} tend to increase soil strength and resistance to deformation by providing electrostatic attraction to multiple particles (Brandenburg and Lagaly, 1988; Markgraf et al., 2012a; Paradelo et al., 2013; Czibulya et al., 2014; Stoppe and Horn, 2018). Our study identified positive but non-significant correlations between *integral z* and Ca^{2+} content (Figure 6b), indicating that this bridging mechanism may provide a minor source of micro-aggregate stability in these soils. We note here that we saturated our samples with distilled water prior to performing the AST analyses, which likely reduced the ionic strength of the soil pore water. This procedure, while following methods used in previous rheological measurements (e.g., Baumgarten et al., 2012; Markgraf et al., 2012), may have masked the ability of calcium Ca^{2+} cations to enhance micro-aggregate stability under more realistic field conditions. Future studies that include controlled ion-exchange or water drainage treatments may help to better isolate how micro-aggregate stability is influenced by solid phase properties versus soil solution characteristics.

Altogether, our study results emphasize that iron and aluminum sesquioxides are particularly important contributors to micro-aggregate stability in systems such as the forested soils of this studied catena. At the same time, microscale properties often reflect macroscale processes (Ghezzehei and Or, 2001; Or and Ghezzehei, 2002). With this concept in mind, we posit that rheological measurements such as the ones used here can help identify soils with inherent stability versus vulnerability to disturbance. Specifically, soils with higher *integral z* values, such as the Alfisol and Mollisol of this study, may better resist erosive processes and have more capacity to sequester and store carbon within stable micro-aggregates. In contrast, soils with lower *integral z* values, such as the studied Inceptisol and Entisol, may be more prone to erosion and degradation.

This information can therefore be used in conjunction with variables such as land use and topography to identify and better manage these potentially vulnerable soils.

6. Summary and Conclusion

~~Amplitude sweep tests (ASTs) made with a parallel-plate rheometer revealed differences in aggregate microstructure and stability along a forested catena. The catena included four soil pedons that varied in the amount of development, with each representing a different soil order: Alfisol (Pedon 1), Mollisol (Pedon 2), Inceptisol (Pedon 3), and Entisol (Pedon 4). The AST curves were translated into parameters including G'_0 (initial elasticity), G''_0 (initial plasticity), γ_L (deformation limit), γ_f (flow point), and *integral z*. These parameters.~~ In this study we used amplitude sweep tests (ASTs) made with a parallel-plate rheometer to quantify differences in micro-aggregate stability along a forested catena with four different soil orders. The rheological parameters enabled quantification of structural stability and aggregation of soils, and revealed significant differences among the pedons. For instance, the Mollisol had relatively high parameter values, thus indicating greater microstructural stability. The Entisol, by contrast, had relatively low parameter values. This soil had the coarsest texture and exhibited the least amount of soil development, thus providing evidence that rheometric measurements are sensitive to differences in soil development.

The *integral z* parameter, which represents the ability of a soil to store energy elastically during deformation, integrates information from the other rheological parameters. Therefore, we used that parameter as the response variable in linear regressions to evaluate how different soil physicochemical properties influence micro-structural stability. That analysis revealed that soil aggregate microstructure and stability were greater in soils with higher clay content, iron and aluminum sesquioxides, and calcium concentrations. At the same time, horizons with moderate to dominant presence of 2:1 phyllosilicate minerals (e.g., smectite and vermiculate) appeared to have relatively high elasticity over a range of deformation, possibly due to the presence of bridging calcium cations in those soils.

Altogether, rheological parameters such as *integral z* appear to be useful indicators for aggregate microstructure and stability. Further, because they provide quantitative information on soil deformation and collapse, these measures can be considered to represent aspects of soil quality. Finally, observed differences between studied horizons and pedons suggest that these parameters may be used to assess relative amount of soil development within – and perhaps across – soil catenas.

Acknowledgments

The authors are grateful to Dr. Dörthe Holthusen from Department of Vegetation Studies, Landscape Management, Federal Institute of Hydrology, Koblenz, Germany for her assistance. The Vali-e-Asr University of Rafsanjan, Iran, is acknowledged for providing facilities. Funding for this work was provided in part by the Virginia Agricultural Experiment Station and the Hatch Program of the National Institute of Food and Agriculture, USDA (1007839).

References

Abid, M., Lal, R. 2009. Tillage and drainage impact on soil quality: II. Tensile strength of aggregates, moisture retention and water infiltration. Soil and Tillage Research, 103(2), 364-372.

Ajayi, A. E., Holthusen, D., Horn, R. 2016. Changes in microstructural behavior and hydraulic functions of biochar amended soils. Soil and Tillage Research, 155, 166–175.

Ajayi, A. E., Horn, R. 2017. Biochar-induced changes in soil resilience: effects of soil texture and biochar dosage. Pedosphere, 27(2), 236-247.

Asgari, N., Ayoubi, S., Demattê, J. A. 2018. Soil drainage assessment by magnetic susceptibility measures in western Iran. Geoderma regional, 13, 35-42.

Baumgarten, W., Dörner, J., Horn, R. 2013. Microstructural development in volcanic ash soils from South Chile. Soil and Tillage Research, 129, 48-60.

Baumgarten, W., Horn, R. 2013. Assessing soil degradation by using a scale-spanning soil mechanical approach: a review. Advances in GeoEcology. Cremlingen: Catena Verlag, 42, 1-61.

Baumgarten, W., Neugebauer, T., Fuchs, E., Horn, R. 2012. Structural stability of Marshland soils of the riparian zone of the Tidal Elbe River. Soil and Tillage Research, 125, 80-88.

Boix-Fayos, C., Calvo-Cases, A., Imeson, A. C., Soriano-Soto, M. D. 2001. Influence of soil properties on the aggregation of some Mediterranean soils and the use of aggregate size and stability as land degradation indicators. Catena, 44(1), 47-67.

Brandenburg, U., Lagaly, G. 1988. Rheological properties of sodium montmorillonite dispersions. Applied Clay Science, 3(3), 263-279.

Buchmann, C., Schaumann, G. E. 2017. Effect of water entrapment by a hydrogel on the microstructural stability of artificial soils with various clay content. Plant and Soil, 414(1-2), 181-198.

Castro Filho, C. D., Lourenço, A., Guimarães, M. D. F., Fonseca, I. C. B. 2002. Aggregate stability under different soil management systems in a red latosol in the state of Parana, Brazil. Soil and Tillage Research, 65(1), 45-51.

Cho, G. C., Dodds, J., Santamarina, J. C. 2006. Particle shape effects on packing density, stiffness, and strength: natural and crushed sands. Journal of Geotechnical and Geoenvironmental Engineering, 132(5), 591-602.

Czibulya, Z., Szegi, T., Michéli, E., Tombácz, E. 2014. Rheological measurements for indicating structural changes in selected soil catenas of European experimental fields. Agriculture Science Technology, 2(1), 22-31.

Dexter, A. R. 1988. Strength of soil aggregates and of aggregate beds in Impact of water and external forces on soil structure. Selected papers of the 1st Workshop on soilphysics and soilmechanics, Hannover 1986. Catena (11), 35-52.

Dixon, J. B., Weed, S. B. 1989. Minerals in soil environments. Soil Science Society of America Inc. (SSSA).

Duiker, S.W., Rhoton, F.E., Torrent, J., Smeck, N.E. and Lal, R., 2003. Iron (hydr) oxide crystallinity effects on soil aggregation. Soil Science Society of America Journal, 67(2), 606-611.

Geological Survey of Iran, 1995. Geological Quadrangle Map. NoI11. Geology Organization of Iran.

Ghezzehei, T. A., Or, D. 2001. Rheological properties of wet soils and clays under steady and oscillatory stresses. Soil Science Society of America Journal, 65(3), 624-637.

Goebel, M. O., Krueger, J., Fleige, H., Igel, J., Horn, R., Bachmann, J. 2017. Frequency dependence of magnetic susceptibility as a proxy for fine-grained iron minerals and aggregate stability of south Chilean volcanic ash soils. Catena, 158, 46-54.

Guo, Z., Zhang, L., Yang, W., Hua, L., Cai, C. 2019. Aggregate Stability under Long-Term Fertilization Practices: The Case of Eroded Ultisols of South-Central China. Sustainability, 11(4), 1169.

Gyawali, A. J., Stewart, R. D. 2019. An improved method for quantifying soil aggregate stability. Soil Science Society of America Journal, 83(1), 27-36.

Holthusen, D., Peth, S., Horn, R. 2010. Impact of potassium concentration and matric potential on soil stability derived from rheological parameters. Soil and Tillage Research, 111(1), 75-85.

Holthusen, D., Reeb, D., Horn, R. 2012. Influence of potassium fertilization, water and salt stress, and their interference on rheological soil parameters in planted containers. Soil and Tillage Research, 125, 72-79.

Husson, O. 2013. Redox potential (Eh) and pH as drivers of soil/plant/microorganism systems: a transdisciplinary overview pointing to integrative opportunities for agronomy. Plant and Soil, 362(1-2), 389-417.

Igwe, C.A., Zarei, M. and Stahr, K., 2013. Stability of aggregates of some weathered soils in south-eastern Nigeria in relation to their geochemical properties. Journal of Earth System Science, 122(5), 1283-1294.

IUSS Working Group WRB. 2015. International Soil Classification System for Naming Soils and Creating Legends for Soil Maps. World Soil Resources Reports No. 106. FAO, Rome.Jackson, M. L. 1958. Soil chemical analysis prentice Hall. Inc., Englewood Cliffs, NJ, 498, 183-204.

Jackson, M. L. 1958. Soil chemical analysis prentice Hall. Inc., Englewood Cliffs, NJ, 498, 183-204.

Jastrow, J. D., Miller, R. M. 1991. Methods for assessing the effects of biota on soil structure. Agriculture, Ecosystems & Environment, 34(1-4), 279-303.

Keller, T., Lamandé, M., Peth, S., Berli, M., Delenne, J. Y., Baumgarten, W., Rabbel, W., Radjai, F., Rajchenbach, J., Selvadurai, A. P. S., Or, D. 2013. An interdisciplinary approach towards improved understanding of soil deformation during compaction. Soil and Tillage Research, 128, 61-80.

Khitrov, N. B., Khaydapova, D. D. 2019. Viscoelastic Behavior of Vertic Solonetz in the Kamennaya Steppe. Eurasian Soil Science, 52(7), 808-821.

Kittrick, J. A., Hope, E. W. 1963. A procedure for the particle-size separation of soils for X-ray diffraction analysis. Soil Science, 96(5), 319-325.

Kottek, M., Grieser, J., Beck, C., Rudolf, B., Rubel, F. 2006. World map of the Köppen-Geiger climate classification updated. Meteorologische Zeitschrift, 15(3), 259-263.

Le Bissonnais, Y.L., 1996. Aggregate stability and assessment of soil crustability and erodibility: I. Theory and methodology. European Journal of soil science, 47(4), 425-437.

Levine, E. R., Ciolkosz, E. J. 1983. Soil development in till of various ages in northeastern Pennsylvania. Quaternary Research, 19(1), 85-99.

Malkin, A. Y., Isayev, A. I. 2017. Rheology: concepts, methods, and applications. Elsevier.

Markgraf, W. 2011. Rheology in soils. Encyclopedia of Agrophysics (Eds J. Glinski, J. Horabik, J. Lipiec). Springer Press, Dordrecht-Heidelberg-London-New York.

Markgraf, W., Horn, R. 2006. 4. Rheometry in soil mechanics: Microstructural changes in a Calcaric Gelysol and a Dystric Planosol. Microstructural Changes in Soils Rheological Investigations in Soil Mechanics, 38, 79.

Markgraf, W., Horn, R. 2007. Scanning electron microscopy–energy dispersive scan analyses and rheological investigations of South-Brazilian soils. Soil Science Society of America Journal, 71(3), 851-859.

Markgraf, W., Horn, R., Gragg, L., Cassell, J. 2009. Rheological investigations in soil micro mechanics: measuring stiffness degradation and structural stability on a particle scale. Progress in management engineering. New York: Nova Science Publishers, 237-79.

Markgraf, W., Horn, R., Peth, S. 2006. An approach to rheometry in soil mechanics-Structural changes in bentonite, clayey and silty soils. Soil and Tillage Research, 91(1-2), 1-14.

Markgraf, W., Watts, C. W., Whalley, W. R., Hrkac, T., Horn, R. 2012. Influence of organic matter on rheological properties of soil. Applied Clay Science, 64, 25-33.

Martin, M. Á., Reyes, M., Taguas, F. J. 2017. Estimating soil bulk density with information metrics of soil texture. Geoderma, 287, 66-70.

Mbagwu, J.S.C. and Schwertmann, U., 2006. Some factors affecting clay dispersion and aggregate stability in selected soils of Nigeria. International agrophysics, 20(1), 23-30.

McKeague, J., Day, J. 1966. Dithionite-and oxalate-extractable Fe and Al as aids in differentiating various classes of soils. Canadian Journal of Soil Science, 46(1), 13-22.

Mehra, O. P., Jackson, M. L. 1958. Iron oxide removal from soils and clays by a dithionite–citrate system buffered with sodium bicarbonate. Clays and clay minerals. Pergamon, 7, 317-327.

Mezger, T. G. 2006. The rheology handbook: for users of rotational and oscillatory rheometers. Vincentz Network GmbH & Co KG.

Muggler, C. C., van Griethuysen, C., Buurman, P., Pape, T. 1999. Aggregation, organic matter, and iron oxide morphology in Oxisols from Minas Gerais, Brazil. Soil Science, 164(10), 759-770.

Nelson, D.W., Sommers, L.E. 1982. Total Carbon, Organic matter. In: Page, A.L., et al. (Ed.), Method of Soil Analysis. Part II. 2nd ed., Agron. Monger. No. 9. ASA and SSSA, Madison, WI, 539– 577.

Ohtsubo, M., Yoshimura, A., Wada, S. I., Yong, R. N. 1991. Particle interaction and rheology of illite-iron oxide complexes. Clays and Clay minerals, 39(4), 347-354.

Or, D., Ghezzehei, T. A. 2002. Modeling post-tillage soil structural dynamics: a review. Soil and Tillage Research, 64(1-2), 41-59.

Paradelo, R., van Oort, F., Chenu, C. 2013. Water-dispersible clay in bare fallow soils after 80 years of continuous fertilizer addition. Geoderma, 200, 40-44.

Pasquini, A. I., Campodonico, V. A., Rouzaut, S., Giampaoli, V. 2017. Geochemistry of a soil catena developed from loess deposits in a semiarid environment, Sierra Chica de Córdoba, central Argentina. Geoderma, 295, 53-68.

Pértile, P., Holthusen, D., Gubiani, P. I., Reichert, J. M. 2018. Microstructural strength of four subtropical soils evaluated by rheometry: properties, difficulties, and opportunities. Scientia Agricola, 75(2), 154-162.

Pértile, P., Reichert, J. M., Gubiani, P. I., Holthusen, D., Costa, A. D. 2016. Rheological parameters as affected by water tension in subtropical soils. Revista Brasileira de ciência do solo, 40.

Pinheiro-Dick, D. and Schwertmann, U., 1996. Microaggregates from Oxisols and Inceptisols: dispersion through selective dissolutions and physicochemical treatments. Geoderma, 74(1-2), 49-63.

Rhoades, J. D. 1996. Salinity: Electrical conductivity and total dissolved solids. Methods of Soil Analysis, Part 3: Chemical Methods, Soil Science Society of America, Madison, WI. 417-435.

Richards, L. A. 1954. Diagnosis and improvement of saline and alkali soils. USDA Handbook No. 60. U.S. Department of Agriculture, Washington, DC.

Rosemary, F., Indraratne, S. P., Weerasooriya, R., Mishra, U. 2017. Exploring the spatial variability of soil properties in an Alfisol soil catena. Catena, 150, 53-61.

Schaetzl, R., Anderson, S., 2005. Soils: Genesis and Geomorphology. Cambridge University, Cambridge, UK.

Schoeneberger, P.J., Wysocki, D.A., Benham, E.C., 2012. Soil survey staff. 2012. Field Book for Describing and Sampling Soils, Version 3.0. Natural Resources Conservation Service, National Soil Survey Center, Lincoln, NE, pp. 9–14.

Six, J., Bossuyt, H., Degryze, S., Denef, K. 2004. A history of research on the link between (micro) aggregates, soil biota, and soil organic matter dynamics. Soil and Tillage Research, 79(1), 7-31.

Six, J., Elliott, E. T., Paustian, K. 2000a. Soil macroaggregate turnover and microaggregate formation: a mechanism for C sequestration under no-tillage agriculture. Soil Biology and Biochemistry, 32(14), 2099-2103.

Six, J., Paustian, K., Elliott, E. T., Combrink, C. 2000b. Soil structure and organic matter I. Distribution of aggregate-size classes and aggregate-associated carbon. Soil Science Society of America Journal, 64(2), 681-689.

Skjemstad, J. O., LeFeuvre, R. P., Prebble, R. E. 1990. Turnover of soil organic matter under pasture as determined by 13C natural abundance. Soil Research, 28(2), 267-276.

Smith, D. W., Reitsma, M. G. 2002. Towards an explanation for the residual friction angle in montmorillonite clay soil. Environmental Geomechanics. EPFL/Centre Midi, Lausanne, Schweiz, 27-44.

Stoppe, N., Horn, R. 2018. Microstructural strength of tidal soils–a rheometric approach to develop pedotransfer functions. Journal of Hydrology and Hydromechanics, 66(1), 87-96.

Sumner, M. E., Miller, W. P. 1996. Cation exchange capacity and exchange coefficients. Methods of Soil Analysis, Part 3: Chemical Methods, Soil Science Society of America, Madison, WI. 1201-1229.

United States. Department of Agriculture. Soil Conservation Service. 2014. Keys to Soil Taxonomy, Twelfth Edition. U.S. Department of Agriculture.

Van Es, H. M., Schindelbeck, R. R. 2003. Field procedures and data analysis for the Cornell sprinkle infiltrometer. Department of Crop and Soil Science Research Series R03-01. soilhealth.cals.cornell.edu.

Walker, A. L. 1983. The effects of magnetite on oxalate-and dithionite-extractable iron. Soil Science Society of America Journal, 47(5), 1022-1026.

Walkley, A., Black, I. A. 1934. An examination of the Degtjareff method for determining soil organic matter, and a proposed modification of the chromic acid titration method. Soil Science, 37(1), 29-38.

Wang, J.G., Yang, W., Yu, B., Li, Z.X., Cai, C.F. and Ma, R.M., 2016. Estimating the influence of related soil properties on macro-and micro-aggregate stability in ultisols of south-central China. Catena, 137, 545-553.

Yoder, R. E. 1936. A direct method of aggregate analysis of soils and a study of the physical nature of erosion losses 1. Agronomy Journal, 28(5), 337-351.

Tables

Table 1. Mean values (n = 3) of physicochemical and morphological properties of the studied pedons[a]

Horizon	Depth (cm)	Clay	Sand	CF	SOC	CCE	CEC ($cmol_+$ kg^{-1})	pH	EC (dS m^{-1})	Ca^{2+} (mmol l^{-1})	Fe_d	Fe_o	Al_o	Bd (g cm^{-3})	rH	Color[b]	SR	ST	Mottles[c]/ Redoximorphic Features[d]
		%									(g kg^{-1})					moist			
Pedon 1: Aeric Endoaqualfs																			
A	0-11	21.7	26.7	10.0	4.2	9.0	26.6	7.10	0.767	15.94	7.6	1.3	4.7	1.23	-	10 YR 5/2	sbk	SiL	m, 4, P, 10 YR 7/8, M, S RMX, m, 3, P, 10 Y 6/1, M, I, MAT, L, S
Btg1	11-38	31.3	17.7	19.2	4.4	15.1	25.0	7.10	0.873	13.53	14.0	4.7	5.3	1.48	16.8	10 YR 5/2	sbk	SiCL	m, 4, P, 10 YR 6/6 & 10 BG, M, S RMX, m, 3, P, 10 Y 6/1, M, I, MAT, L, S
Btg2	38-125	13.0	36.0	20.0	0.6	27.7	22.6	7.33	0.870	15.33	13.4	5.5	5.8	1.56	17.2	10 BG 5.5/1	sbk	L	m, 4, P, 10 YR 8/8 & 10 BG, M, S RMX, m, 3, P, 10 Y 6/1, M, I, MAT, L, S
Pedon 2: Aquic Argiudolls																			
Oi	0-8	22.3	34.0	47.6	13.6	0.2	27.2	5.10	0.473	9.4	18.3	3.1	5.5	0.61	-	7.5 YR 2.5/1	-	-	-
AB	8-39	25.33	26.7	31.9	5.7	0.5	22.0	6.30	0.877	14.2	15.7	7.2	6.2	1.20	-	10 YR 3/3	sbk	CL	-
Btg1	39-80	60.0	6.3	58.1	0.8	3.1	23.7	5.63	0.680	10.9	16.6	7.1	6.0	1.26	14.8	5 G 5/1	sbk	C	RMX, f,1, D,10YR3/3, M, I, MAT, L, S
Btg2	80-120	54.3	8.7	60.0	0.5	1.5	22.5	6.03	0.457	11.2	15.5	5.5	6.0	1.57	15.7	6 G 5/1	sbk	C	RMX, c, 2, D, 10 YR 3/3, M, I, MAT, L, S
Pedon 3: Oxyaquic Eutrudepts																			
A1	0-4	32.0	34.3	53.0	11.8	4.2	28.3	6.07	0.433	10.3	4.7	2.4	2.4	0.67	-	7.5 YR 2.5/3	cr	CL	-
A2	4-15	34.3	33.7	41.5	8.3	12.7	28.0	6.93	0.837	13.7	4.3	2.6	2.4	1.25	-	7.5 YR 2/3	gr	CL	-
Bw	15-28	32.7	42.0	44.4	0.8	20.2	25.5	7.27	0.433	15.4	3.8	1.5	0.9	1.53	-	7.5 YR 5/3	sbk	CL	c, 2, D, 7.5 YR 5/8 & 5 G 6/1, M, S
Bg1	28-45	20.3	53.0	43.2	0.5	21.2	24.6	7.30	0.430	14.8	3.2	3.0	0.8	1.62	21.4	10 GY 5/1	sbk	SCL	c, 2, D, 7.5 YR 5/8 & 5 G 6/1, M, S
Bg2	45-59	18.3	52.7	56.7	0.9	10.9	24.9	7.23	0.540	16.3	5.3	5.0	1.1	1.69	21.5	10 GY 5/1	sbk	SL	m, 3, P, 7.5 YR 5/8 & 5 G 6/1, M, S
2Bw1	59-75	34.3	26.7	32.1	1.6	2.7	31.0	6.83	0.633	14.0	10.5	9.6	8.3	1.28	-	7.5 YR 3/3	sbk	C	m, 4, P, 7.5 YR 5/8 & 5 G 6/1, M, S

2Bw2	75-125	52.3	23.0	31.5	0.8	1.6	31.4	6.80	0.653	14.1	9.5	7.6	5.5	1.48	-	7.5 YR 4/3	sbk	C	c, 2, D, 7.5 YR 5/8 & 5 G 6/1, M, S
Pedon 4: Mollic Endoaquents																			
A	0-15	11.7	41.0	41.41	12.9	18.8	27.4	7.03	0.853	10.9	6.0	4.4	2.4	1.20	-	7.5 YR 2/3	gr	L	-
Ckg1	15-41	11.0	52.3	49.38	3.2	30.5	16.5	7.03	0.567	7.8	2.5	2.1	0.3	1.54	22.4	10 YR 5/2	m	SL	m, 2, P, 7.5 YR 5/8 & 5 G 6/1, M, S
Ckg2	41-63	14.7	56.0	56.42	1.0	32.0	20.3	7.33	0.707	13.8	3.1	0.8	0.2	1.52	21.1	7.5 YR 7.5/1	m	SL	m, 2, P, 7.5 YR 5/8 & 5 G 6/1, M, S
R	63+	-	-	-	-	-	-	-	-	-	-	-	-	-	-		-	-	-

[a] Soils classification is based on the Soil Taxonomy system (Soil Survey Staff, 2014).

[b] Color: Used standard Munsell® notation from the "Soil Color" section

Note: coarse fragments (CF); soil organic carbon (SOC); calcium carbonate equivalent (CCE); cation exchange capacity (CEC); sodium adsorption ratio (SAR); electrical conductivity (EC); soluble calcium (Ca^{2+}); dithionite-citrate-extractable Fe (Fe_d); oxalate-extractable Fe and Al (Fe_o and Al_o); bulk density (Bd); saturation percentage (SP); reducing condition (rH)

- = Not detected

Soil structure (SR): crumb (cr), granular (gr), massive (m), subangular blocky (sbk)

Soil texture (ST): Clay (C), Loam (L), Clay Loam (CL), Sandy Loam (SL), Silty Loam (SiL), Sandy Clay Loam (SCL), Silty Clay Loam (SiCL)

[c] Mottles: few (f), common (c), m (many), fine (1), medium (2), coarse (3), very coarse (4), distinct (D), prominent (P), moist (M), spherical (S)

[d] Redoximorphic Features: reduced matrix (RMX), few (f), common (c), many (m), fine (1), medium (2), coarse (3), distinct (D), predominant (P), moist (M), irregular (I), in the matrix (not associated with peds/pores) (MAT), loose (L), sharp (S)

Table 2. Clay mineralogy of selected soil horizons of studied pedons, based on Dixon and Weed guideline (1989). D = Dominant (≥25%); M = Moderate (10-25%); T = Trace (<10%); - = Not detected.

Horizon	Phyllosilicate clay minerals assemblage
	Pedon 1: Alfisol
A	Kaolinite (D), Smectite (M), Vermiculite (M), Illite (M), Quartz (T)
Btg1	Kaolinite (D), Smectite (M), Vermiculite (M), Illite (T), Quartz (T)
Btg2	Kaolinite (D), Smectite (M), Vermiculite (M), Illite (T), Quartz (T)
	Pedon 2: Mollisol
AB	Vermiculite (D), Illite (M), Kaolinite (M), Smectite (T), Chlorite (T), Quartz (T)
Btg1	Smectite (D), Kaolinite (M), Vermiculite (M), Illite (M), Quartz (M), Chlorite (T)
Btg2	Smectite (D), Kaolinite (M), Quartz (M), Illite (M), Chlorite (T), Vermiculite (T)
	Pedon 3: Inceptisol
A1	Kaolinite (D), Quartz (M), Vermiculite (T), Smectite (T)
A2	Kaolinite (D), Quartz (M), Vermiculite (T), Smectite (T)
Bw	Kaolinite (D), Quartz (D), Smectite (T)
Bg1	Kaolinite (D), Smectite (M), Quartz (M), Illite (T)
Bg2	Kaolinite (D), Smectite (M), Quartz (M), Vermiculite (T), Illite (T)
2Bw1	Kaolinite (D), Smectite (D), Quartz (M), Illite (M), Vermiculite (T), Chlorite (T)
2Bw2	Kaolinite (D), Smectite (D), Quartz (M), Illite (M), Vermiculite (T), Chlorite (T)
	Pedon 4: Entisol
A	Kaolinite (M), Vermiculite (M), Illite (M), Smectite (T), Quartz (T)
Ckg1	Quartz (D), Kaolinite (M), Illite (M), Vermiculite (T)
Ckg2	Quartz (D), Kaolinite (M), Illite (M), Vermiculite (T)

Table 3. Summarized results from amplitude sweep tests with controlled shear deformation (n = 5). Values indicate mean ± standard deviations. G'_0 = storage modulus at 0 % deformation; G''_0 = loss modulus at 0 % deformation; γ_L = deformation limit (last value within a linear viscoelastic range); γ_f = flow point is given in terms of deformation percentage; *integral z* is defined by Eq. (2) and quantifies microstructural elasticity. Different lower case letters indicate significant differences in parameter values ($p < 0.05$).

Horizon	G'_0 (kPa)	G''_0 (kPa)	γ_L (%)	γ_f (%)	*integral z*
			Pedon 1: Alfisol		
A	1350 ± 14 c	224 ± 9.3 c	0.013 ± 0.001 b†	33.6 ± 5.5 bc	23.4 ± 4.7 bc
Btg2	7190 ± 268 ab	1120 ± 141 a	0.025 ± 0.006 b†	46.8 ± 6.6 ab	68.3 ± 6.2 a
			Pedon 2: Mollisol		
AB	5150 ± 423 ab	605 ± 10 b	0.024 ± 0.000 a†	22.7 ± 4.2 cd	28.0 ± 6.2 b
Btg1	5880 ± 424 ab	1280 ± 305 a	0.043 ± 0.006 a†	55.2 ± 6.4 a	82.8 ± 7.3 a
			Pedon 3: Inceptisol		
A2	8020 ± 131 a	1530 ± 532 a	0.012 ± 0.001 b†	11.7 ± 2.7 de	14.4 ± 5.0 bc
Bg1	6290 ± 181 b‡	735 ± 73 b‡	0.025 ± 0.002 b†	18.0 ± 8.0 d‡	8.1 ± 2.4 bc‡
2Bw2	2560 ± 202 b‡	517 ± 50 b‡	0.032 ± 0.002 b†	22.4 ± 3.5 d‡	27.4 ± 1.4 bc‡
			Pedon 4: Entisol		
A	265 ± 7 d	63.7 ± 5.5 d	0.014 ± 0.001 b†	15.1 ± 1.5 de	19.0 ± 1.6 bc
Ckg1	55.4 ± 6.2 e	13.6 ± 1.1 e	0.025 ± 0.002 b†	4.2 ± 1.3 e	7.2 ± 1.2 c

†γ_L was only analyzed for differences at the pedon level because interactions were not significant for that parameter ($p > 0.05$)
‡Bg1 and 2Bw2 horizons in Pedon 3 were grouped together as subsoil in the statistical analysis

Figures

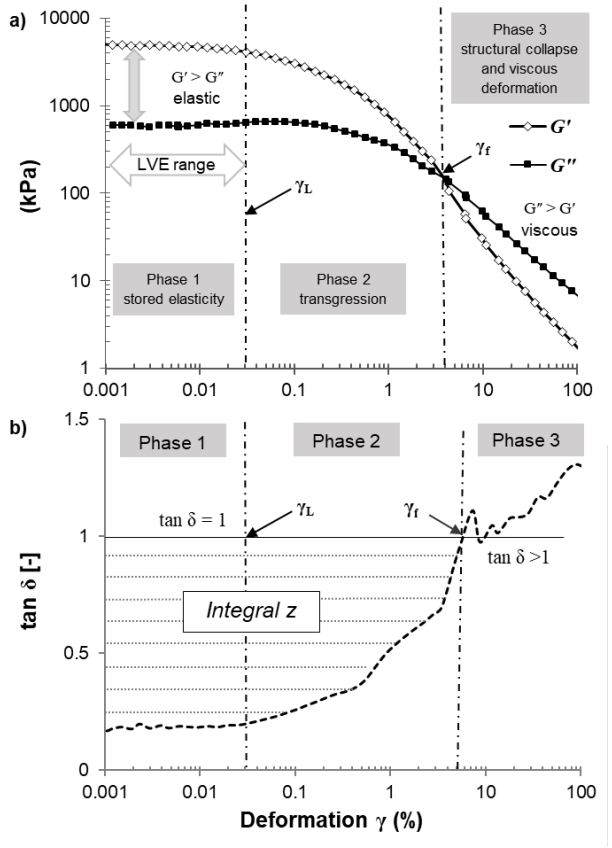

Fig. 1. Representative results from an amplitude sweep test (AST) with controlled shear deformation. a) G′ (storage modulus) and G″ (loss modulus) versus deformation γ, divided into 1) quasi-elastic stage, which is defined by the linear viscoelastic (LVE) range, 2) transgression phase, bounded by the deformation limit (γ_L) and flow point (γ_f), and 3) viscous phase. B) loss factor tan δ (G″/ G′) versus deformation γ; when tan δ > 1 the medium becomes vicious. Material stiffness is related to *integral z* (indicated by dashed line and calculated by Equation [2]).

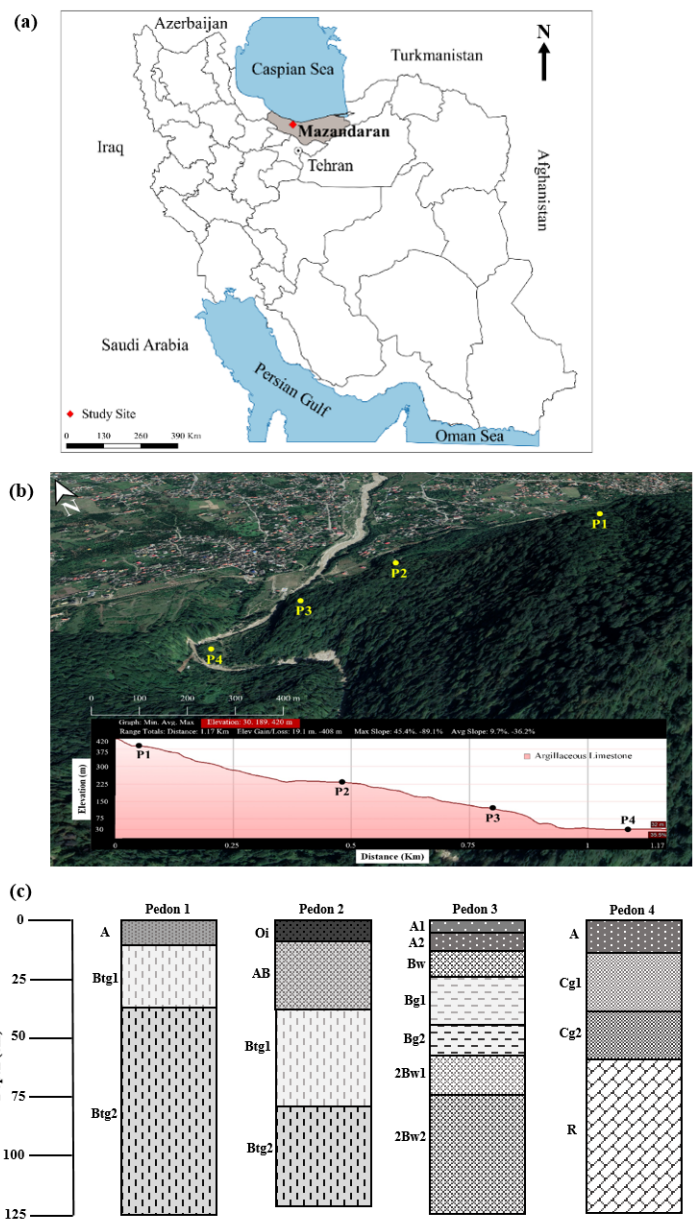

Fig. 2. a) Location of the study site in the north of Iran; b) overview of Kehyrud forest along with the locations and elevations of the four studied pedons along the hillslope catena; and c) genetic horizons for the studied pedons. P1 = Pedon 1, P2 = Pedon 2, P3 = Pedon 3, and P4 = Pedon 4.

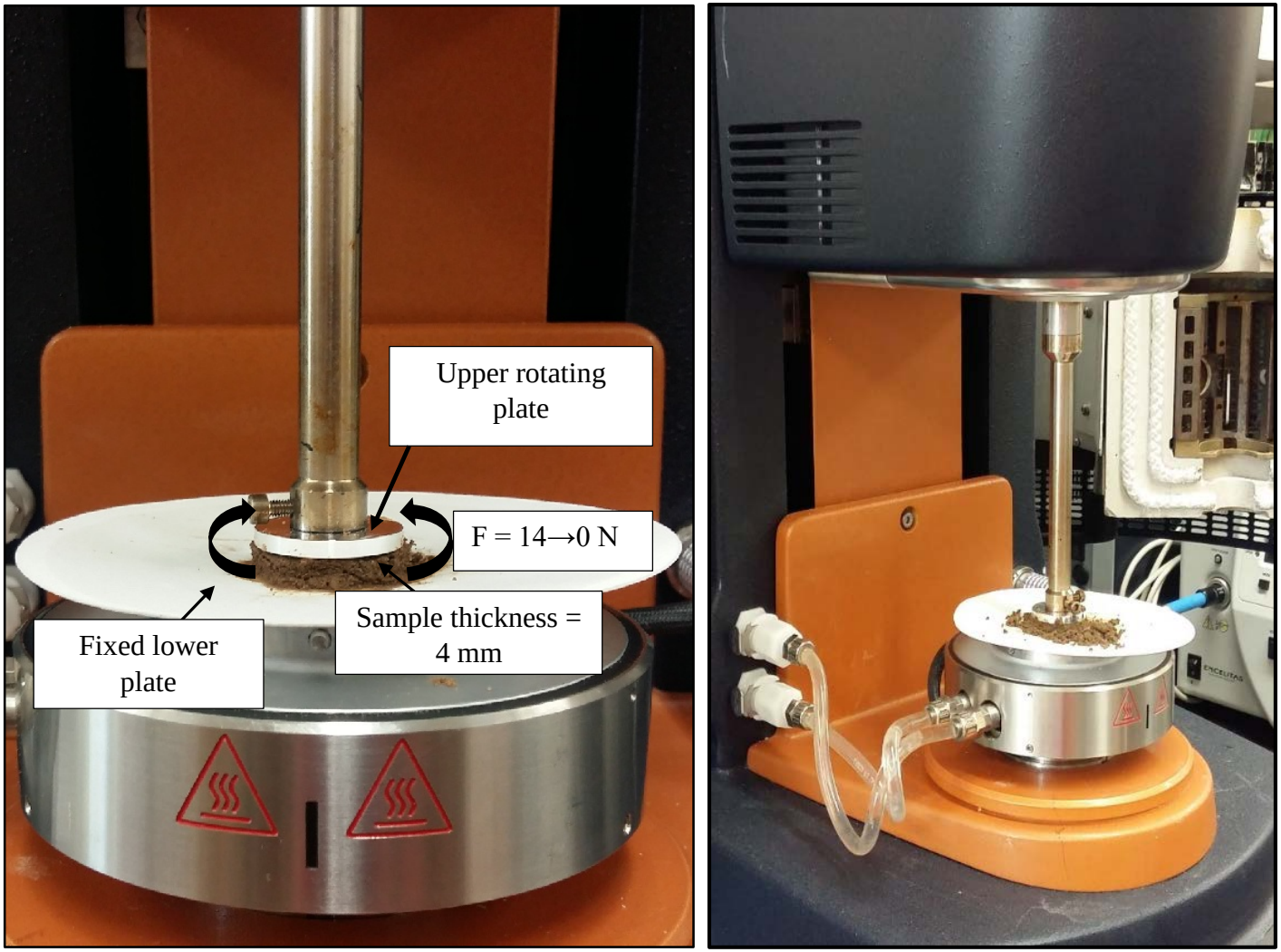

Fig. 3. Rheometer and measuring system of parallel plates for an amplitude sweep test (AST) with controlled shear deformation. The soil samples were prepared with the normal force (F) from 14 N (starting) to 0 N (ending) and a gap between plates (i.e., sample thickness) of 4 mm. The panel on the right shows a sample at the end of the test.

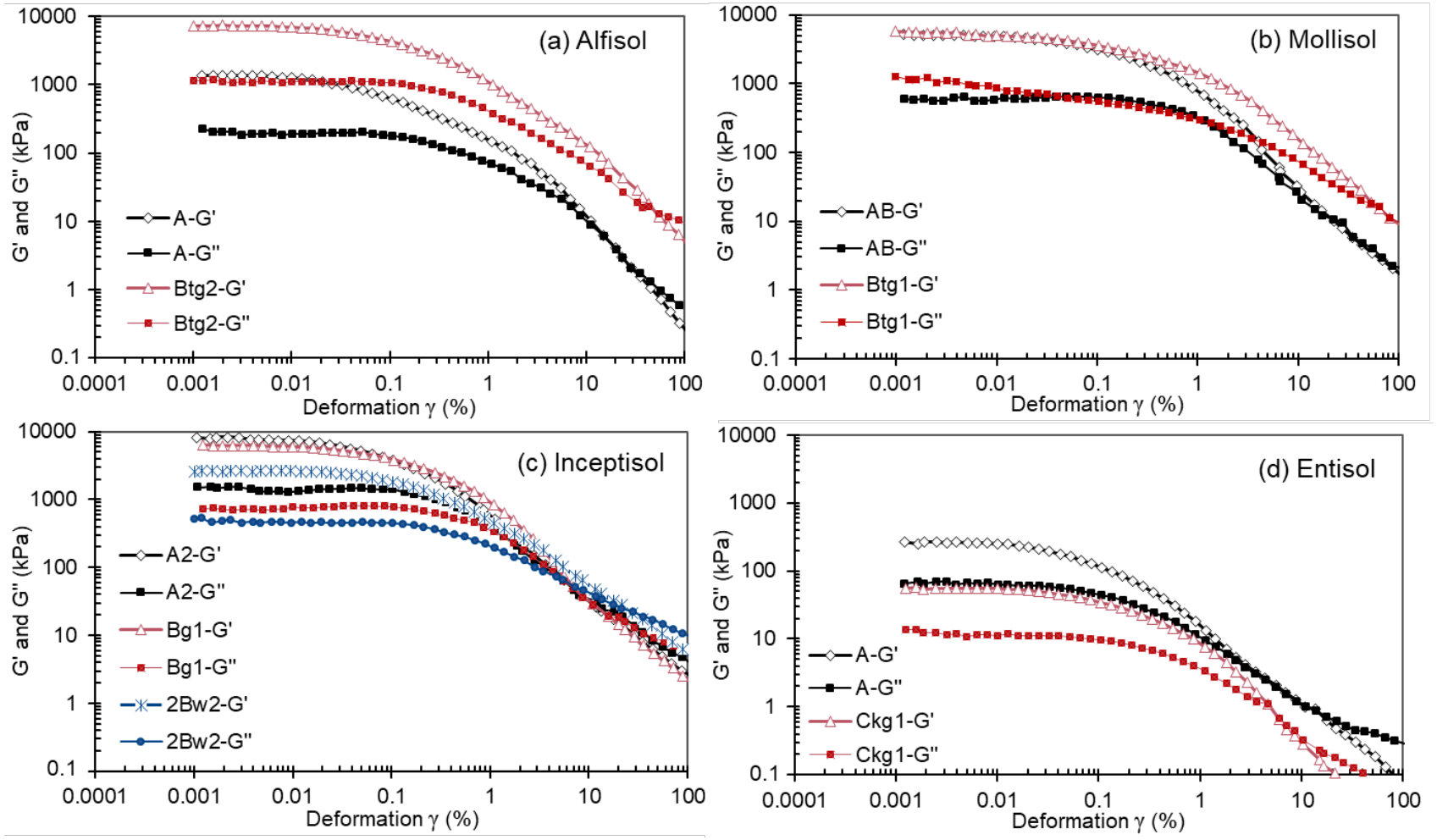

Fig. 4. Results of amplitude sweep test (AST) under oscillatory and controlled shear deformation with (distilled water) saturated samples, indicating mean values for storage modulus (G′), loss modulus (G″), deformation (γ) of the studied pedons.

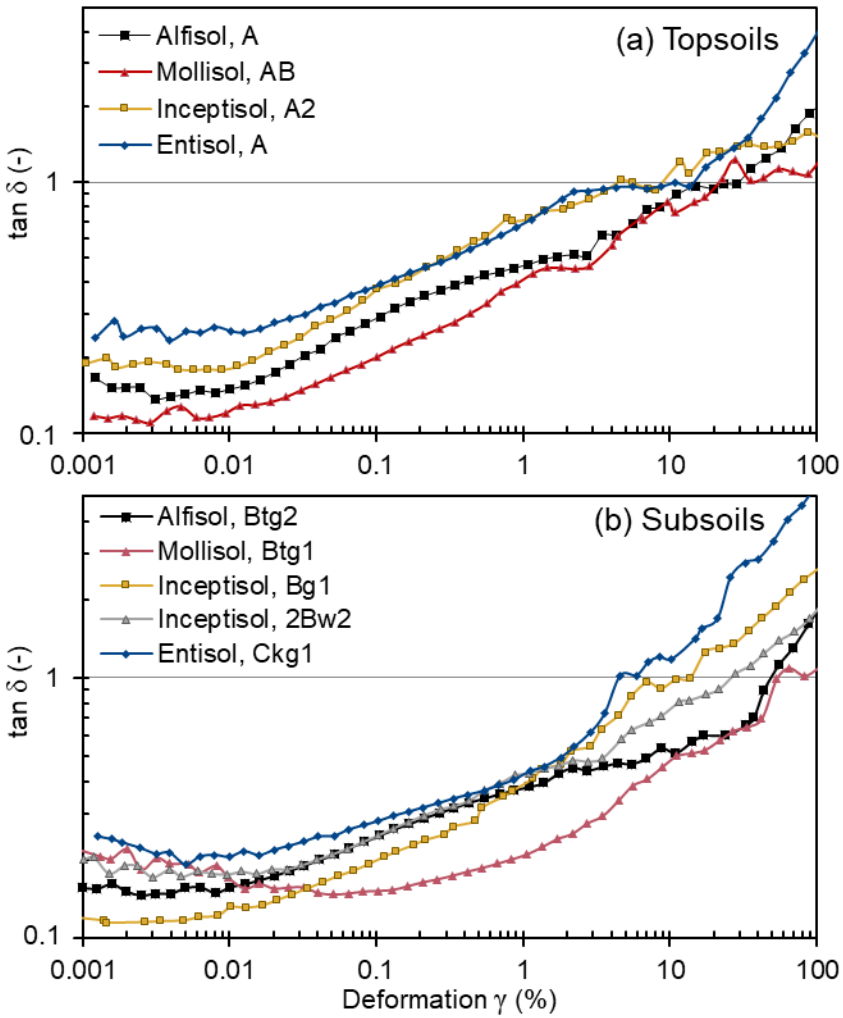

Fig. 5. Mean values of tan δ at different deformation γ for each (a) topsoil and (b) subsoil genetic horizon. Curves were derived from amplitude sweep tests (ASTs) under oscillatory and controlled shear deformation.

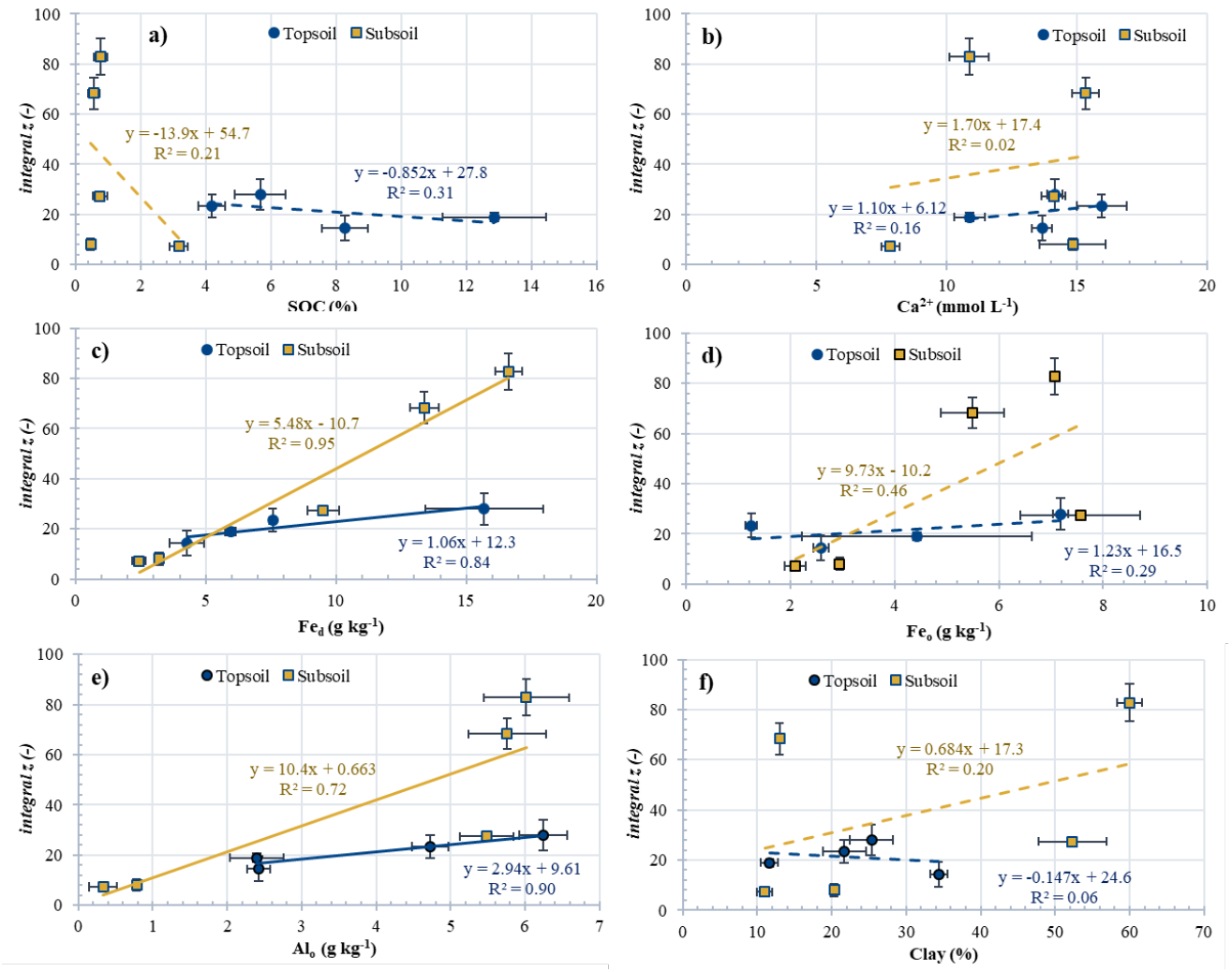

Fig. 6. Correlations of *integral z* in topsoil versus subsoil samples with: (a) soil organic carbon (SOC); (b) calcium (Ca^{2+}); (c) dithionite-citrate extractable iron (Fe_d); (d) acid ammonium oxalate extractable iron (Fe_o); (e) acid ammonium oxalate extractable aluminum (Al_o); and (f) clay percentage. Points represent mean values and error bars indicate standard deviations. Solid lines indicate significant regression slopes ($p < 0.1$), whereas dashed lines indicate non-significant slopes.